# Characterization of Microstructures Fabricated by Two-Photon Polymerization Using Coherent Anti-Stokes Raman Scattering Microscopy

**Tommaso Baldacchini,*,† Maxwell Zimmerley,‡ Chun-Hung Kuo,† Eric O. Potma,‡ and Ruben Zadoyan†**

*Technology and Applications Center, Newport Corporation, Irvine, California 92606, and Department of Chemistry, University of California, Irvine, California 92697*

*Received: June 23, 2009; Revised Manuscript Received: August 5, 2009*

We demonstrate the possibility to image microstructures fabricated by two-photon polymerization (TPP) using coherent anti-Stokes Raman scattering (CARS) microscopy. The imaging contrast based on chemical selectivity attained by CARS microscopy is used to gather qualitative information on TPP. Upon the basis of detailed knowledge of the characteristic signatures of the photoresist Raman spectrum, quantitative relationships between laser writing conditions and polymer cross-linking are demonstrated. The increase in degree of polymer conversion as a function of laser average power follows a sigmoidal profile which is interpreted in terms of a simple model based on the polymerization mechanism of the photoresist.



## I. Introduction

In two-photon polymerization (TPP), near-infrared photons are employed to pattern photoresists in a "spot-by-spot" writing fashion. Although most photoresists are transparent in the near-infrared region of the spectrum, excitation is induced through two-photon absorption by employing ultrashort pulsed lasers and by using high numerical aperture objective lenses. The large photon densities attained under these conditions allow polymerization to take place exclusively within the focal volume of the excitation laser beam, producing volume elements (voxels) on the order of femtoliters. Hence, three-dimensional structures with almost no topological constraints and with submicrometer resolution can be easily manufactured by overlapping voxels in predetermined patterns. After fabrication, the microstructures are revealed by washing away the unpolymerized portion of the photoresist with an organic solvent.[1]

TPP has a unique advantage over more conventional microfabrication techniques in that it permits exploring the effects of substrate topology on several phenomena in a way nearly impossible to accomplish otherwise. This is most evident in the field of photonic crystals, where microstructures with complex three-dimensional periodicity such as diamond-like, spiral, quasi-crystal, and slanted-pore lattices have all been successfully fabricated.[2−6] By adjusting the period length and lattice-type of photonic crystals, the flow of light can be controlled through these microstructures in extraordinary manners. Furthermore, TPP has been shown to be a key manufacturing method for the realization of devices in fields as diverse as bioengineering, microelectronics, and microelectromechanical systems.[7−10] Thus, despite the relatively slow processing time that accompanies it, TPP is a prominent addition to the growing arsenal of advanced microfabrication techniques available to researchers.

Since the inception of TPP,[11−13] several improvements have been implemented that widen the variety of devices that can be created using this method. For example, with the introduction of clever electroless plating and inversion procedures, the organic-base scaffold of microstructures fabricated by TPP can be converted into semiconductive and conductive materials.[14,15] In addition, two approaches have been shown to be effective in reducing processing time. In the first, a microlens array is used instead of a conventional objective lens to fabricate several structures at once.[16] In the second approach, microtransfer molding is used to quickly stamp many replicas of a master structure created by TPP.[17] Writing resolution though is undoubtedly the aspect of TPP that has evolved most rapidly over time. Early observations of the existence of intensity thresholds below which no polymerization is induced hinted that breaking the diffraction limit could be possible.[18] In fact, by optimizing the writing parameters, voxels with diameters smaller than 100 nm can now be easily formed.[19,20] Furthermore, in a recent report, resolution 20 times smaller than the wavelength of the excitation laser beam was achieved producing voxels as small as 40 nm.[21]

Despite these recent technical advances, understanding at a molecular level of how experimental conditions influence the ultimate mechanical properties of microstructures fabricated by TPP is still incomplete. This information is essential for the incorporation of TPP-fabricated microstructures in functional devices. For instance, the Young's modulus and glass transition of polymers patterned by TPP with feature sizes less than a micrometer were measured, the results being considerably smaller than those measured for the corresponding bulk materials.[22,23] Such observations indicate that, depending on the TPP conditions used for microfabrication, different degrees of material cross-linking can bring about material properties in the microstructure that deviate significantly from those of the bulk material. While control of the degree of polymerization in the voxel during the actual writing process is of the utmost importance for further improving TPP, it has been a challenge to directly measure the level of chemical conversion in the focal plane.

Measuring the polymerization process during TPP puts some specific demands on a potential probing technique. First, the method needs to be sensitive to the degree of chemical conversion. Second, the probing time should be compatible with the relevant time scale of TPP, which is in the range of

* Corresponding author. E-mail: tommaso.baldacchini@newport.com.
† Newport Corporation.
‡ University of California.

10.1021/jp9058998 CCC: $40.75 
Published on Web 08/31/2009

microsecond to millisecond per voxel. Third, the probing volume needs to colocalize with the voxel addressed in TPP. These requirements allude to an optical probing technique with molecular selectivity and a sufficiently high spatial resolution.

In this work, we explore the use of coherent anti-Stokes Raman scattering (CARS) microscopy as a potential diagnostic tool for characterizing the chemical changes in microstructures fabricated by TPP. CARS microscopy has been a successful imaging technique in biological and biomedical research.[24] Recently, the CARS approach has also been used to visualize engineered materials such as polymer blends,[25,26] liquid crystals,[27,28] and thin film photoresists.[29] CARS microscopy derives its analytical capability from the Raman active modes of molecules. Unlike spontaneous Raman scattering, CARS signals can be collected at very high acquisition rates, down to the microsecond time scale. In addition, the three-dimensional probing volume in CARS microscopy resembles the voxel size in TPP. Most importantly, CARS signals can be detected on the same platform used for TPP manufacturing, offering opportunities for simultaneous writing and probing during microfabrication. Here we show that CARS microscopy provides rapid characterization of the degree of polymerization of a typical photoresist used in TPP. These results demonstrate the diagnostic potential of CARS microscopy in rapidly analyzing written patterns in the native photoresist.



## II. Materials and Methods

A detailed description of the experimental setups employed for TPP and CARS microscopy can be found elsewhere.[30,31] Briefly, TPP excitation is provided by a Ti:sapphire laser delivering 100 fs pulses at a repetition rate of 80 MHz and with center wavelength of 775 nm (MaiTai DeepSee, Spectra-Physics). The laser beam is focused into the photoresist by means of a 40× microscope objective lens with a numerical aperture of 0.75. During microfabrication, the excitation focal point is kept fixed, while the sample is moved in predetermined geometries with the aid of a computer-controlled, motorized, three-axis translation stage assembly (XMS, Newport Corp.). The characteristic average laser power and writing speed used for TPP are 5 mW and 10 $\mu$m/s, respectively.

For CARS microscopy, a synchronously pumped optical parametric oscillator (OPO) system is used as the light source. The Stokes beam at 1064 nm is delivered by a 76 MHz, 7 ps Nd:Vanadate laser (PicoTrain, High-Q Laser), while the pump beam is produced by the OPO (Levante Emerald, APE) which can be tuned from 760 to 960 nm. This light source provides broad tunability (1000−3500 $cm^{-1}$ Stokes shifts) and high spectral resolution (2−5 $cm^{-1}$). The CARS signal is generated in the photoresist by matching the frequency difference between pump and Stokes beams to the frequency of a Raman active vibrational mode of the sample. CARS spectra are obtained by scanning the frequency of the pump beam. The beams are focused by a 40×, water immersion objective lens with a numerical aperture of 1.15. Typical illumination powers at the samples are ~10 mW per beam. Imaging is achieved by raster-scanning the focal spot using a galvanometric mirror pair (Fluoview 300, Olympus) and detecting the spectrally filtered CARS signal with a photomultiplier tube (Hamamatsu, R-3896). In this study, only the forward propagating CARS signal was collected.

The photoresist employed for TPP consists of three components homogenously mixed together, resulting in a viscous liquid that can be applied onto flat glass substrates by either spin or drop casting.[32] A Norrish type I photoinitiator (Irgacure 369, Ciba) makes up 3% of the photoresist, while the remainder is equally divided between two trifunctional acrylic monomers (SR499 and SR368, Sartomer). Molecular structures of the photoinitiator and both monomers are shown in Figure 1(a−c). Upon two-photon absorption, the photoinitiator generates two radicals through a unimolecular reaction in which the bond between the carbonyl group and the tertiary carbon atom breaks homolytically. The two newly formed radicals initiate polymerization of the monomers through a chain reaction mechanism. During the propagation step of this process, the carbon−carbon double bonds of the monomers are quickly consumed generating an interconnected network of monomers linked by carbon−carbon single bonds, a polymer. Immediately after excitation, the molecular weight of the polymer grows with the successive additions of excess monomer units. A series of termination processes though slow down the polymerization until no more new carbon−carbon single bonds can be formed.[33] In addition, since our photoresist is not degassed before use molecular oxygen dissolved in the sample plays an important deactivation role in the polymerization process.[34]

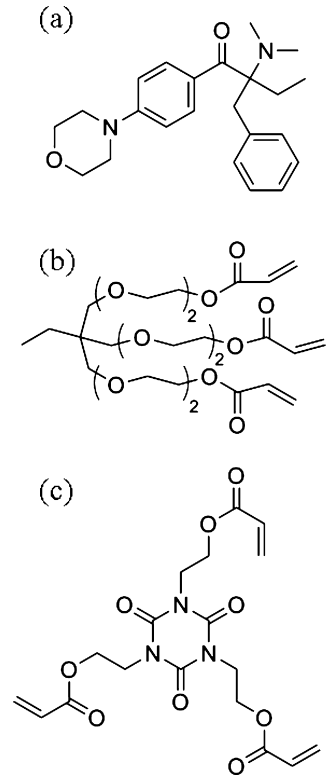


**Figure 1.** Molecular structures of the photoresist components used for TPP: the photoinitiator (a) Irgacure 369 and the two acrylic monomers (b) SR499 and (c) SR368.

## III. Results and Discussion

**A. Chemical Imaging in the Range between 2800 and 3000 $cm^{-1}$.** As a result of the high density of aliphatic and aromatic carbon−hydrogen bonds, organic materials exhibit strong signals in their Raman spectra in the 3000 $cm^{-1}$ range. The photoresist employed in this study contains an abundance of these modes (Figure 1), permitting visualization of microstructures fabricated by TPP with excellent vibrational contrast. We fabricated a tower 20 $\mu$m tall, and with sides 30 $\mu$m long. To enhance its adhesion to the glass substrate, a layer of polymer only a few micrometers thick was fabricated between the substrate and the tower. A scanning electron micrograph of this

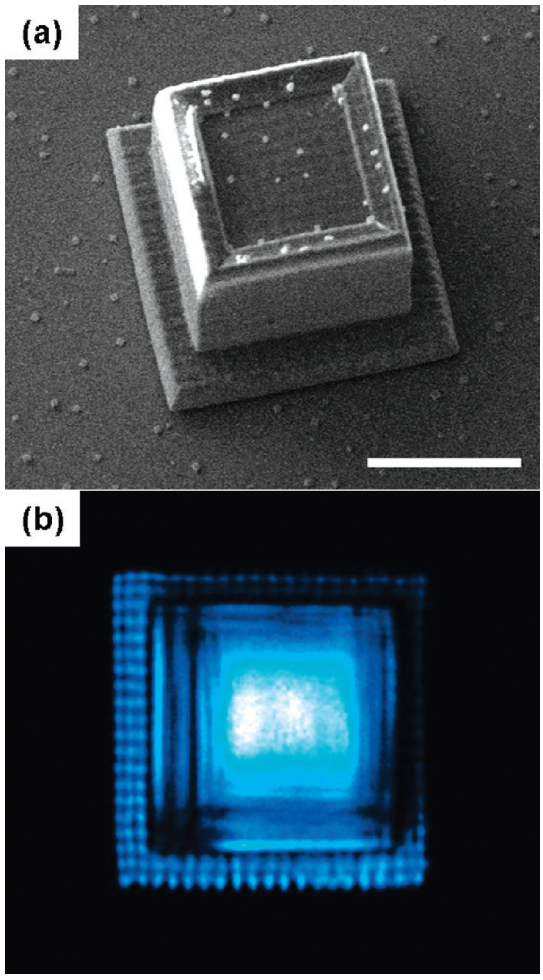


**Figure 2.** Three-dimensional microstructure fabricated by TPP. (a) Tilted view of the microstructure obtained by scanning electron microscopy. The scale bar is 20 $\mu$m. (b) Background corrected CARS image of the microstructure at 2900 cm$^{-1}$. The image represents a cross-section of the microstructure at a height of 5 $\mu$m above the substrate. Only a resonant signal contributes to the formation of the image.



microstructure is presented in Figure 2(a). The image was acquired with the sample tilted to show the three-dimensionality of the object.

The central region, walls, and base of the microstructure were created by using identical microfabrication conditions (excitation wavelength, laser average power, stage velocities, focusing lens) with the exception of the "writing" patterns used to make them. The central part of the tower was created by overlapping layers in the axial direction every 2 $\mu$m. Each layer consisted of a raster-scan pattern 22 $\mu$m wide and long, with a separation between lines of 0.1 $\mu$m. The walls of the tower were fabricated in the axial direction in the same way as the central part of the tower with each layer composed of eight concentric squares written at a separation of 0.5 $\mu$m. This procedure resulted in a set of walls 4 $\mu$m thick, 30 $\mu$m long, and 20 $\mu$m tall. Finally, the layer of polymer used as an adhesion promoter was fabricated by raster-scanning a pattern with a separation between lines of 0.8 $\mu$m in both the vertical and horizontal directions. This part of the microstructure consisted of only one layer.

Figure 2(b) shows the CARS image of the same microstructure. It is a section recorded at a height of 5 $\mu$m above the glass substrate. As a consequence, no contribution to the signal generation is observed arising from the glass. Furthermore, the image in Figure 2(b) is the pure resonant signal of the microstructure.[35] It was obtained by subtracting the image acquired at 2900 cm$^{-1}$, which is on resonance with the carbon−hydrogen stretching mode of the polymer, with the image acquired at 2750 cm$^{-1}$, far away from any Raman active modes of the polymer. Hence, the contrast observed in Figure 2(b) depends exclusively on differences of the resonant contribution of the material to the CARS signal.

Figure 2(b) shows CARS imaging of all three parts that constitute the microstructure. A stronger signal is observed at the center of the image corresponding to the area of the tower fabricated with the highest density of laser passes. Weaker and more inhomogeneous signals arise from the walls of the towers and its base where a smaller number of laser passes were used to create them than were used for creating the center of the tower. The TPP pattern employed in the fabrication of the tower base resulted in the gridlike, periodic signal in the CARS image. Since the CARS signal is strongly dependent on the number of vibrational oscillators,[24] discontinuities in the image in Figure 2(b) are a direct consequence of the density variations of the material. The denser the material, the higher the concentration of carbon−hydrogen bonds that give rise to stronger CARS signals.

Although three-dimensionality and surface roughness of the microstructure can be imaged by scanning electron microscopy, CARS imaging unambiguously indicates that its density is not homogeneous throughout. Thus, CARS microscopy in the carbon−hydrogen stretching vibrational region is a useful method for mapping density variations in microstructures fabricated by TPP. In particular, optimization of TPP can be achieved by exploring the effect of laser or sample scanning strategies used to create a microstructure on its density once the size of the voxel is set.

**B. Chemical Imaging in the Range between 1500 and 1750 cm$^{-1}$.** Raman spectra of a film of the photoresist before and after UV polymerization are shown in Figure 3(a). Three distinctive peaks at 1595, 1635, and 1720 cm$^{-1}$ are observed. They are assigned to the aromatic ring vibration of the photoinitiator, the monomers carbon−carbon double bond stretching, and the monomers carbonyl group stretching, respectively.[36] Since the concentration of carbon−carbon double bonds diminishes during polymerization, the peak intensity at 1635 cm$^{-1}$ becomes smaller as a consequence. The other two peaks should stay unaltered based on the fact that neither the aromatic ring of the photoinitiator nor the carbonyl group of the monomers participates in the polymerization reaction. Although this is true for the lower wavenumber peak, a change in intensity and shift to longer wavenumber are observed for the peak at 1720 cm$^{-1}$. This is not attributed to a change in concentration of carbonyl groups but instead to a change in its local environment. The carbonyl moiety of the acrylic ester unit is indeed in conjugation with the carbon−carbon double bond. When this bond disappears during polymerization, the conjugation is broken and hence induces a change in the carbonyl group vibrational mode.[37]

CARS spectra of the unpolymerized photoresist and of a microstructure fabricated using 16 mW laser average power are shown in Figure 3(b) in the frequency range between 1550 and 1750 cm$^{-1}$. Characteristic dispersive line shapes are observed for all three Raman active modes of the photoresist present in this region of the spectrum, with the signal at 1635 cm$^{-1}$ being the strongest. Moreover, cross-linking of the monomers by TPP considerably reduces the intensity of the carbon−carbon double bond CARS signal. Since the intensity of the CARS signal is proportional to the square modulus of the material third-order nonlinear susceptibility ($\chi^{(3)}$), quantitative information on the

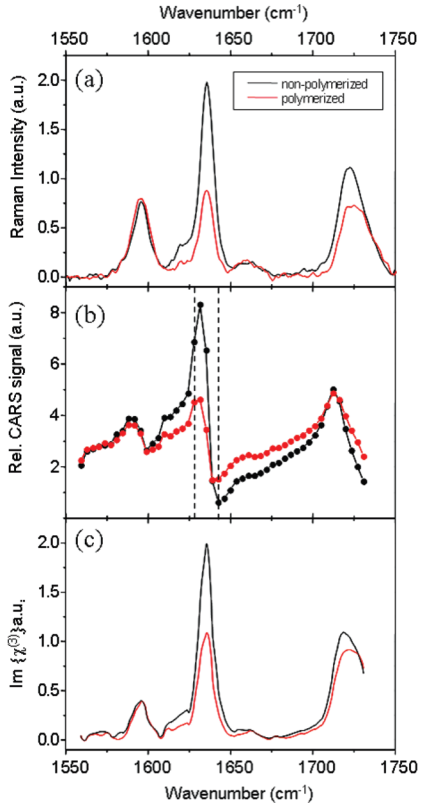


**Figure 3.** Difference in vibrational spectra between unpolymerized (black) and polymerized (red) photoresist. (a) Raman spectra of the photoresist before and after UV polymerization. (b) CARS spectra of the photoresist before and after TPP. CARS spectra are normalized to the signal of the glass substrates on top of which TPP was performed. Vertical dashed lines at 1628 and 1643 $cm^{-1}$ represent the positions in the CARS spectra of the polymerized and unpolymerized photoresist where an inversion in relative intensities occurs. (C) Extracted Im$\{\chi^{(3)}\}$-amplitude from (b) using MEM. In retrieving the spectra, the spectral background phase was subtracted according to the procedure outlined in ref 38.

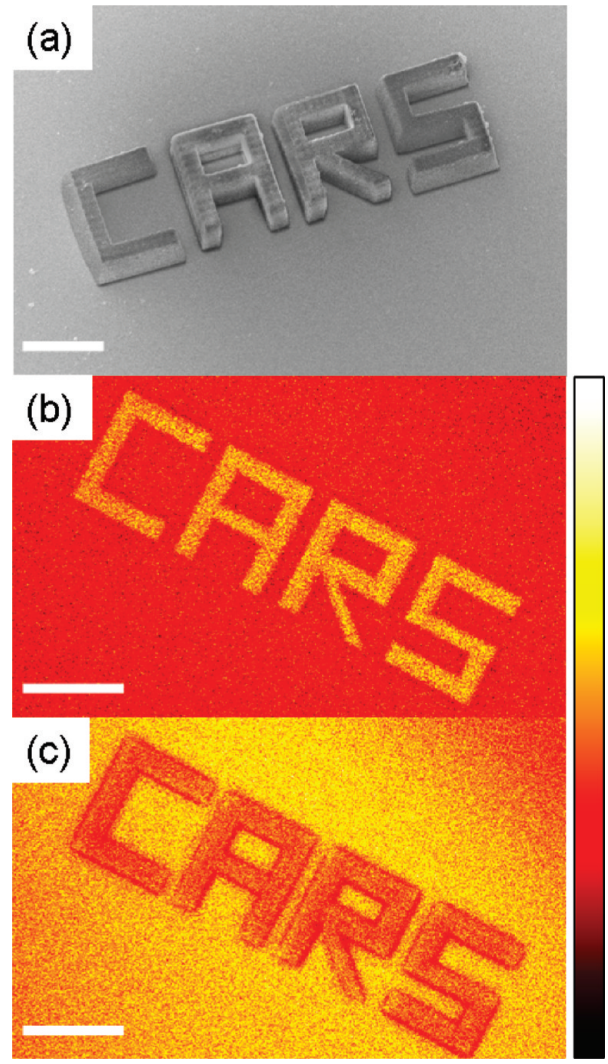


**Figure 4.** (a) Tilted view of a microstructure fabricated by TPP acquired by means of scanning electron microscopy. CARS microscopy was performed on the same microstructure before washing away the unpolymerized portion of the photoresist. Obvious differences are observed if the image is recorded at (b) 1643 $cm^{-1}$ or (c) 1628 $cm^{-1}$ (LUT shown on far right). The relative strengths of the CARS signals originating from the unpolymerized photoresist and the polymerized microstructure get inverted by switching wavenumbers. Figures (b) and (c) are *xy* sections of the microstructure immersed in the unpolymerized photoresist recorded at a height of 5 $\mu$m from the surface of the glass substrate to which the microstructure is attached. The scale bars in (a), (b), and (c) are 20 $\mu$m.

vibrational oscillators responsible for that signal cannot be directly extrapolated from CARS spectra. Therefore, we have implemented the maximum entropy method (MEM) to retrieve the imaginary part only of $\chi^{(3)}$ from CARS spectra.[38] The amplitude of Im$\{\chi^{(3)}\}$ is proportional to the spontaneous Raman spectrum. MEM was applied to the CARS spectra in Figure 3(b), and the retrieved Im$\{\chi^{(3)}\}$ spectra are shown in Figure 3(c). The frequency positions of the signal peaks are in excellent agreement with the vibrational bands of the Raman spectrum. With the exception of the peak at 1595 $cm^{-1}$, the signals' relative intensities also overlap quite well between the spectra in Figures 3(a) and (c). Although the concentrations of the monomers in the photoresist used in TPP were almost identical to the one used for Raman spectroscopy, the concentration of the photoinitiator was different. These results show that CARS measurements can provide information analogous to the concentration-dependent signal intensities attained in Raman spectroscopy, with the important difference that CARS microscopy can provide such information at much higher acquisition rates.

A qualitative example of the fast chemical imaging capability is shown in Figure 4. The dispersive spectral line shape of the CARS signal can be used to generate images with enhanced chemical contrast based on a particular bond vibration. To discriminate polymerized from unpolymerized material, a comparison between images taken at the 1628 $cm^{-1}$ peak and the blue-shifted dip at 1643 $cm^{-1}$ is highly instructive. On the basis of the CARS spectra in Figure 3(b), inverted contrast is expected when comparing images taken at these spectral positions (vertical lines in Figure 3(b)), offering a direct and quick procedure for visualizing polymerized material without the necessity of removing the unpolymerized portion of the sample. To prove this point, the word CARS was written by TPP onto a glass substrate. Each letter was 20 $\mu$m wide, 25 $\mu$m long, and 10 $\mu$m tall. An image of this microstructure recorded with an electron microscope is shown in Figure 4(a). While still immersed in the bath of unpolymerized photoresist, the same microstructure was imaged by CARS microscopy. Images with completely reversed contrast were obtained when the Raman shift was tuned from 1643 to 1628 $cm^{-1}$. At 1643 $cm^{-1}$, shown in Figure 4(b), the signal from the microstructure is stronger than the signal from the unpolymerized photoresist, while at 1628 $cm^{-1}$, shown in Figure 4(c), the signal from the unpoly-

merized photoresist is stronger than the signal from the microstructure.

**C. Microstructure Degree of Conversion.** The area of a peak in a Raman spectrum is proportional to the concentration of the oscillators responsible for that particular Raman active mode. Thus, spectra such as the one in Figure 3(a) can be used to measure the degree of conversion (DC) in photoresists following polymerization. For acrylic-based photoresists, DC represents the number of carbon−carbon double bonds consumed during polymerization and is a major factor influencing the mechanical properties of polymers. The higher the DC, the stronger the polymer. Since the number of carbonyl groups in the photoresist remains the same before and after polymerization, the peak at 1720 $cm^{-1}$ can be used as an internal reference for DC estimation.[39] The percentage of DC is obtained using the following equation

$$DC = \left[1 - \left(\frac{A_{C=C}}{A_{C=O}} \middle/ \frac{A'_{C=C}}{A'_{C=O}}\right)\right] \times 100 \qquad (1)$$

where $A_{C=C}$ and $A_{C=O}$ are the integrated intensities of the carbon−carbon double bond and of the carbon−oxygen double bond peaks in the polymerized photoresist, respectively, while $A'_{C=C}$ and $A'_{C=O}$ are the integrated intensities of the same peaks in the unpolymerized photoresist. A thin film of the photoresist used in this study was fully cured by UV illumination, and its DC was measured to be 45%. This number is comparable to DC values measured for other fully cured acrylic-based photoresists that are composed of highly branched monomers.[40] Both monomers in our photoresist contain three sites where polymerization can take place. Hence, a highly cross-linked network is formed during polymerization that can severely limit molecular mobility. The probability that an unreacted carbon−carbon double bond will encounter a radical is dramatically reduced with the evolving polymerization, and a complete conversion (DC = 100%) is never reached.

To investigate how different writing conditions affect DC in microstructures created by TPP, a set of test samples were prepared and investigated by CARS microscopy. The sample consisted of an array of towers that were all fabricated with the same writing conditions with the exception of laser average power. This was varied from 8 to 16 mW. Each tower was 12 $\mu$m tall, and it had a square cross-section with sides 10 $\mu$m long. CARS microscopy was performed on these microstructures while still immersed in the unpolymerized photoresist. In one image then, we could measure the CARS signal strengths of both polymerized and unpolymerized photoresist. By tuning the pump beam spectrally with a step size of 4 $cm^{-1}$, we collected CARS spectra of the different parts of the sample processed by TPP. CARS signals were all normalized to the nonresonant signal from the glass coverslip that was used as substrate for the microfabrication process.

CARS spectra of microstructures fabricated by TPP with different laser average powers and corresponding Raman spectra retrieved by MEM are shown in Figures 5(a) and (b), respectively. With increasing energy doses, a gradual decrease in the strength of the peak at 1635 $cm^{-1}$ is observed. The concentration of the monomer carbon−carbon double bond in the patterned photoresist is lower when higher laser average powers were used.

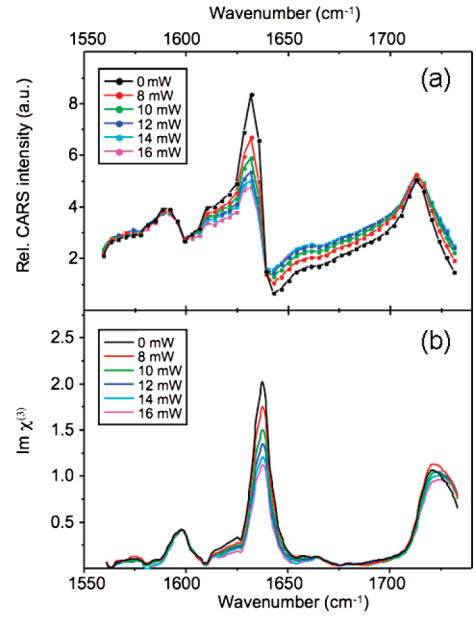


**Figure 5.** (a) CARS spectra of microstructures fabricated by TPP with different laser average powers and (b) extracted Im$\{\chi^{(3)}\}$-amplitude using MEM. The spectra recorded at a laser average power of 0 mW correspond to the signal of the unpolymerized photoresist.

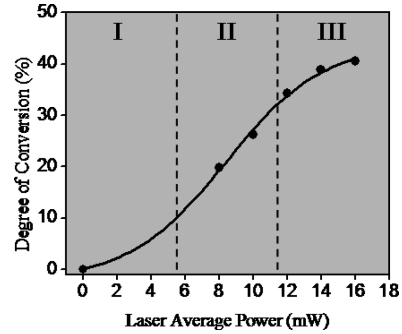


**Figure 6.** Degree of conversion of the photoresist patterned by TPP as a function of laser average power. The value at 0 mW corresponds to the unpolymerized photoresist. The roman numerals indicate the three steps of polymerization mechanism characteristic of multifunctional acrylic monomers (see text). Data were fitted to a sigmoid function to guide the eye.

The spectra in Figure 5(b) were used in combination with eq. 1 to compute DC values of microstructures fabricated by TPP under different writing conditions. The results are illustrated in Figure 6 where DC percentages are plotted against laser average powers. The data are consistent with a model describing the polymerization mechanism of highly branched acrylic monomers which has been well-characterized through kinetics investigations in photoresists similar to the one employed in this study.[41] This model can be illustrated in Figure 6 by a sigmoidal profile where three distinctive regions can be identified. At low laser average powers (region I) DC grows very slowly, indicating that not enough radicals are formed to initiate polymerization. This barrier is due to the presence of molecular oxygen in and around the photoresist. By quenching the triplet state of the photoinitiator and by efficiently scavenging primary radicals, molecular oxygen inhibits radical polymerization. Increasing laser average powers (region II) to the degree that the number of radicals generated by TPP exceeds the number of oxygen molecules in the photoresist, polymerization can occur, and DC values increase rapidly. Finally, for laser average powers larger than 11 mW (region III), diffusion becomes the

dominant factor in both propagation and termination mechanisms of polymerization slowing down the rate at which DC values increase with increasing laser average powers. The size and interconnectivity of the macromolecules formed among monomers during polymerization at this point become so imposing as to forbid any mobility, leading to the presence of a plateau in Figure 6. Although more points might be needed for a precise estimate, it is evident that DC larger that 50% cannot be reached by TPP. This number is in agreement with the value of DC attained by linear polymerization of a thin film of the same photoresist.

The most common strategy employed to increase resolution in TPP is to utilize laser intensities slightly above the threshold required for inducing polymerization.[42] This is usually achieved by setting a low laser average power and by modifying exposure times to obtain the desired writing resolution. Although voxels of different sizes can in effect be created by following this procedure, the results in Figure 4 reveal that the cross-linking of these voxels is also affected. Therefore, the mechanical properties of microstructures fabricated by TPP depend on the writing resolution used to form them. Once the correlation between DC and Young's modulus in a photoresist is established, plots such as the one in Figure 6 can be used to tailor the mechanical properties of a microstructure fabricated by TPP.

This example shows that CARS microscopy can provide quantitative information on the TPP process. On the basis of the quantitative relation between the relative CARS signal at 1635 $cm^{-1}$ and the degree of conversion established here, corrected CARS images of the microstructure can now be directly related to DC. Since CARS images with relative vibrational contrast can be rapidly acquired, this approach allows for an expeditious assessment of the degree of conversion in three-dimensional microstructures.

## IV. Conclusions

We have demonstrated that CARS microscopy is an effective method for characterizing microstructures fabricated by TPP. Establishing a correlation between writing conditions and polymer cross-linking was possible by investigating the photoresist CARS signals around 1635 $cm^{-1}$ that correspond to the stretching mode of the monomer carbon−carbon double bond. This method though is not limited to acrylic-based photoresist only. In combination with Raman spectroscopy, we anticipate that CARS microscopy can be successfully used to characterize TPP of a wide variety of photoresists. Furthermore, the fast acquisition rate in CARS microscopy makes this imaging technique particularly suitable as an in situ, real-time diagnostic tool for TPP.

**Supporting Information Available:** Volume rendering of three-dimensional microstructures fabricated by TPP, obtained by CARS microscopy at around 3000 and 1635 $cm^{-1}$. This material is available free of charge via the Internet at http://pubs.acs.org.

## References and Notes

(1) LaFratta, C. N.; Fourkas, J. T.; Baldacchini, T.; Farrer, R. A. *Angew. Chem., Int. Ed.* **2007**, *46*, 6238.

(2) Cumpston, H. B.; Ananthavel, P. S.; Barlow, S.; Dyer, L. D.; Ehrlich, E. G.; Erskine, L. L.; Heikal, A. A.; Kuebler, M. S.; Sandy Lee, I. Y.; McCord-Maughon, D.; Qin, J.; Röckel, H.; Rumi, M.; Wu, X. L.; Marder, R. S.; Perry, W. J. *Nature* **1999**, *398*, 51.

(3) Kaneko, K.; Sun, H. B.; Duan, X. M.; Kawata, S. *Appl. Phys. Lett.* **2003**, *83*, 2091.

(4) Seet, K. K.; Mizeikis, V.; Matsuo, S.; Juodkazis, S.; Misawa, H. *Adv. Mater.* **2005**, *17*, 541.

(5) Ledermann, A.; Cadematiri, L.; Hermatschweiler, M.; Toninelli, C.; Ozin, G. A.; Wiersma, D. S.; Wegener, M.; von Freymann, G. *Nat. Mater.* **2006**, *5*, 942.

(6) Deubel, M.; Wegener, M.; Kaso, A.; John, S. *Appl. Phys. Lett.* **2004**, *85*, 1895.

(7) Pitts, D. J.; Campagnola, J. P.; Epling, G. A.; Goodman, L. S. *Macromolecules* **2000**, *33*, 1514.

(8) Tayalia, P.; Mendonca, C. R.; Baldacchini, T.; Mooney, D. J.; Mazur, E. *Adv. Mater.* **2008**, *20*, 4494.

(9) Farrer, R. A.; LaFratta, C. N.; Praino, J.; Naughton, M. J.; Saleh, B. E. A.; Teich, M. C.; Fourkas, J. T. *J. Am. Chem. Soc.* **2006**, *128*, 1796.

(10) Maruo, S.; Ikuta, K.; Korogi, H. *Appl. Phys. Lett.* **2003**, *82*, 133.

(11) Strickler, J. S.; Webb, W. W. *Proc. SPIE* **1990**, *1398*, 107.

(12) Wu, E. S.; Strickler, J. H.; Harrell, W. R.; Webb, W. W. *Proc. SPIE* **1992**, *1674*, 776.

(13) Maruo, S.; Nakamura, O.; Kawata, S. *Opt. Lett.* **1997**, *22*, 132.

(14) Tétreault, N.; von Freymann, G.; Deubel, M.; Hermatschweiler, M.; Pérez-Willard, F.; John, S.; Wegener, M.; Ozin, G. A. *Adv. Mater.* **2006**, *18*, 457.

(15) Chen, Y. S.; Tal, A.; Torrance, D. B.; Kuebler, S. M. *Adv. Funct. Mater.* **2006**, *16*, 1739.

(16) Kato, J. I.; Takeyasu, N.; Adachi, Y.; Sun, H. B.; Kawata, S. *Appl. Phys. Lett.* **2005**, *86*, 044102.

(17) LaFratta, C. N.; Baldacchini, T.; Farrer, R. A.; Fourkas, J. T.; Teich, M. C.; Saleh, B. E. A.; Naughton, M. J. *J. Phys. Chem. B* **2004**, *108*, 11256.

(18) Kawata, S.; Sun, H. B.; Tanaka, T.; Takada, K. *Nature* **2001**, *412*, 697.

(19) Takada, K.; Sun, H. B.; Kawata, S. *Appl. Phys. Lett.* **2005**, *86*, 071122.

(20) Haske, W.; Chen, V. W.; Hales, J. M.; Dong, W.; Barlow, S.; Marder, S. R.; Perry, J. W. *Opt. Express* **2007**, *15*, 3426.

(21) Li, L.; Gattass, R. R.; Gershgoren, E.; Hwang, H.; Fourkas, J. T. *Science* **2009**, *324*, 910.

(22) Nakanishi, S.; Shoji, S.; Kawata, S.; Sun, H. B. *Appl. Phys. Lett.* **2007**, *91*, 063112.

(23) Nakanishi, S.; Yoshikawa, H.; Shoji, S.; Sekkat, Z.; Kawata, S. *J. Phys. Chem. B* **2008**, *112*, 3586.

(24) Evans, C. L.; Xie, S. *Annu. Rev. Anal. Chem.* **2008**, *1*, 883.

(25) Lim, S. H.; Caster, A. G.; Nicolet, O.; Leone, S. R. *J. Phys. Chem. B* **2006**, *110*, 5196.

(26) von Vacano, B.; Meyer, L.; Motzkus, M. *J. Raman Spectrosc.* **2007**, *38*, 916.

(27) Kachynski, A. V.; Kuzmin, A. N.; Prasad, P. N.; Smalyukh, I. I. *Appl. Phys. Lett.* **2007**, *91*, 151905.

(28) Saar, B. G.; Park, H. S.; Xie, X. S.; Lavrentovitch, D. O. *Opt. Express* **2007**, *15*, 13585.

(29) Potma, O. E.; Xie, X. S.; Muntean, L.; Preusser, J.; Jones, D.; Ye, J.; Leone, R. S.; Hinsberg, D. W.; Schade, W. *J. Phys. Chem. B* **2004**, *108*, 1296.

(30) Baldacchini, T.; Zimmerley, M.; Potma, O. E.; Zadoyan, R. *Proc. SPIE* **2009**, *7201*, 72010Q–1.

(31) Zimmerley, M.; McClure, A. R.; Choi, B.; Potma, O. E. *Appl. Opt.* **2009**, *48*, D79.

(32) Baldacchini, T.; LaFratta, C. N.; Farrer, R. A.; Teich, M. C.; Saleh, B. E. A.; Naughton, M. J.; Fourkas, J. T. *J. Appl. Phys.* **2004**, *95*, 6072.

(33) Odian, G. *Principles of Polymerization*; Wiley: New York, 1991.

(34) Studer, K.; Decker, C.; Beck, E.; Schwalm, R. *Prog. Org. Coat.* **2003**, *48*, 92.

(35) Baldacchini, T.; Zadoyan, R. *Laser Focus World* **2009**, 45 May.

(36) Esen, C.; Kaiser, T.; Schweiger, G. *Appl. Spectrosc.* **1996**, *50*, 823.

(37) Newport Corp.; *Application Note 42* (www.newport.com).

(38) Vartiainen, E. M.; Rinia, H. A.; Müller, M.; Bonn, M. *Opt. Express* **2006**, *14*, 3622.

(39) Houbertz, R.; Domann, G.; Schulz, J.; Olsowski, B.; Fröhlich, L. *Appl. Phys. Lett.* **2004**, *84*, 1105.

(40) Decker, C. *Nucl. Instrum. Methods Phys. Res., Sect. B* **1999**, *151*, 22.

(41) Selli, E.; Bellobono, I. R. Photopolymerization of Multifunctional Monomers: Kinetic Aspects. In *Radiation Curing in Polymer and Technology*; Fouassier, J. P., Rabek, J. F., Eds.; Elsevier: New York, 1993; Vol. III, pp 1−32.

(42) Ovsianikov, A.; Chichkov, B. N. Two-Photon Polymerization - High Resolution 3D Laser Technology and Its Applications. In *Nanoelectronics and Photonics*; Korkin, A., Rosei, F., Eds.; Springer: New York, 2008; pp 427−446.

JP9058998